IEEE Access
Multidisciplinary ⋮ Rapid Review ⋮ Open Access Journal

Received 12 February 2023, accepted 5 April 2023, date of publication 11 April 2023, date of current version 18 April 2023.

Digital Object Identifier 10.1109/ACCESS.2023.3266288

RESEARCH ARTICLE

An Efficient Application of Turbo Coding for OFDM In-Phase/Quadrature Index Modulation

EUNCHUL YOON, (Senior Member, IEEE), SOONBUM KWON, AND SUN YONG KIM, (Senior Member, IEEE)
Department of Electrical and Electronics Engineering, Konkuk University, Seoul 05029, South Korea

Corresponding author: Sun Yong Kim (kimsy@konkuk.ac.kr)

This research was supported by Basic Science Research Program through the National Research Foundation of Korea (NRF) funded by the Ministry of Education (2018R1D1A1B07050232, 2021R1F1A1047578).

ABSTRACT We present a method to efficiently apply turbo coding to OFDM in-phase/quadrature index modulation (OFDM-IQ-IM) for both cases of presence and absence of puncturing. We show that using the posterior probabilities of turbo-coded bits in the Bahl-Cocke-Jelinek-Raviv (BCJR) decoding algorithm yields the same decoding performance as using the likelihood probabilities of turbo-coded bits. We investigate the difference in error rate between systematic bits and parity check bits of systematic turbo coding and the difference in error rate between index selecting bits (ISBs) and symbol selecting bits (SSBs) of OFDM-IQ-IM. Based on the results, we devise a new bit mapping scheme that can efficiently split turbo-coded bits into ISBs and SSBs in OFDM-IQ-IM. Simulations show that the proposed bit mapping scheme improves the bit error rate (BER) of the turbo-coded 4QAM-based OFDM-IQ-IM approach and that the turbo-coded 4QAM-based OFDM-IQ-IM approach applying the proposed bit mapping scheme outperforms the turbo-coded 4QAM-based OFDM approach in the high signal-to-noise ratio (SNR) region.

INDEX TERMS Turbo decoding, in-phase/quadrature index modulation, interleaving, puncturing.

I. INTRODUCTION

Index modulation (IM) is a promising technology that can achieve additional transmission rates by using indices of an active resource, where the resource can be a transmission entity such as transmit antenna, subcarrier, modulation type, precoder, time slot, channel status, etc [1], [2]. The concept of IM was applied to orthogonal frequency division multiplexing (OFDM) to be known as OFDM-IM [3], [4]. To further improve the spectral efficiency of OFDM-IM, numerous variants of OFDM-IM such as OFDM in-phase/quadrature IM (OFDM-IQ-IM), dual-mode OFDM-IM (DM-OFDM-IM), multiple-mode OFDM-IM (MM-OFDM-IM), and layered OFDM-IM (L-OFDM-IM) have been developed [5], [6], [7], [8], [9], [10], [11]. Note that an early concept similar to IQ-IM can be found in quadrature spatial modulation [12], [13]. To enhance the bit error rate (BER) performance of OFDM-IM, numerous OFDM-IM variants such as coordinate interleaved OFDM-IM (CI-OFDM-IM), enhanced CI-OFDM-IM (ECI-OFDM-IM), linear constellation precoding OFDM-IQ-IM (LCP-OFDM-IQ-IM), and generalized MM-OFDM-IM (GMM-OFDM-IM) have been developed [7], [14], [15], [16]. Recent OFDM-IM variant techniques incorporating the IQ concept can be found in [17] and [18]. In [19], a Gray-coded index mapping was adopted as an efficient mapping between the index selecting bit (ISB) sequences and constellation mode pattern (CMP) sequences for a small subblock size of DM-OFDM-IM. In [20], the concept of efficient mapping was extended to large subblock sizes of OFDM-IQ-IM and CI-MM-OFDM-IM. A low-density parity check (LDPC) code was applied to OFDM-IM in [21] and to MM-OFDM-IM in [22]. Therein, formulas were provided to calculate the posterior probabilities of the ISBs and symbol selecting bits (SSBs) of OFDM-IM, and those probabilities were used as input to the LDPC decoder. However, the application of the formulas was limited in the cases of small subblock sizes and low modulation orders due to computational complexity. In [23], low complexity formulas were derived to calculate the posterior probabilities of the ISBs and SSBs of OFDM-IM, reducing the implementation complexity of

The associate editor coordinating the review of this manuscript and approving it for publication was Shuangqing Wei.

LDPC decoding in LDPC-coded OFDM-IM systems without performance loss. In [24], a factor graph based generalized approximate message passing (G-AMP) algorithm was applied for LDPC decoding in OFDM-IM. LDPC decoding of [24] was based on the posterior probabilities of zero and non-zero symbols transmitted on inactive and active subcarriers, resulting in decoding complexity that increases exponentially with symbol constellation size. In [25], iterative channel estimation and data detection based on an AMP algorithm was applied to a turbo receiver of OFDM-IM. However, the joint design of channel estimator, data detector, and channel decoder for the iterative AMP algorithm in [25] inevitably increased the hardware cost and computational complexity. The issues of hardware cost and computational complexity will be mitigated if the turbo decoder design can be decoupled from the OFDM-IM demodulator design. However, to the best of our knowledge, this kind of disjoint design for a turbo-coded OFDM-IM system or its variant has not been reported in the literature. Motivated by the efficient application of turbo coding to OFDM-IM or its variant, this paper focuses on the decoupled design of an OFDM-IQ-IM demodulator and a turbo decoder. As a representative turbo decoding algorithm, the Bahl-Cocke-Jelinek-Raviv (BCJR) decoding algorithm [26] that applies maximum a posteriori decoding has been used. The BCJR decoding algorithm requires the likelihood probabilities of turbo-coded bits as input, whereas the LDPC decoding algorithm often uses the posterior probabilities of LDPC-coded bits as input. Since the ISBs and SSBs of OFDM-IQ-IM are intertwined due to the nature of the IM application, it is very difficult to directly calculate the likelihood probabilities of the turbo-coded bits in OFDM-IQ-IM. Therefore, applying turbo coding to OFDM-IQ-IM may require finding another type of input to the BCJR decoding algorithm instead of the likelihood probabilities of the turbo-coded bits.

In this paper, we present a method to efficiently apply turbo coding to OFDM-IQ-IM for both cases of presence and absence of puncturing. We show that using the posterior probabilities of turbo-coded bits in the BCJR decoding algorithm yields the same decoding performance as using the likelihood probabilities of turbo-coded bits. We investigate the difference in error rate between systematic bits and parity check bits of systematic turbo coding and the difference in error rate between ISBs and SSBs of OFDM-IQ-IM. Based on the results, we devise a new bit mapping scheme that can efficiently split turbo-coded bits into ISBs and SSBs in OFDM-IQ-IM. Simulations show that the proposed bit mapping scheme improves the BER of the turbo-coded 4QAM-based OFDM-IQ-IM approach and that the turbo-coded 4QAM-based OFDM-IQ-IM approach applying the proposed bit mapping scheme outperforms the turbo-coded 4QAM-based OFDM approach in the high signal-to-noise ratio (SNR) region.

The rest of this paper is organized as follows. Section II describes the turbo-coded OFDM-IQ-IM approach. Section III investigates the error rate difference between the systematic bit and parity check bit of systematic turbo coding and the error rate difference between the ISB and SSB of OFDM-IQ-IM, and describes the random bit mapping schemes. Based on the findings, Section III describes the proposed bit mapping schemes for both cases of presence and absence of puncturing. Section V shows by simulation that the proposed bit mapping scheme outperforms a random bit mapping scheme when applied for a turbo-coded OFDM-IQ-IM approach. Finally, Section VI provides concluding remarks.

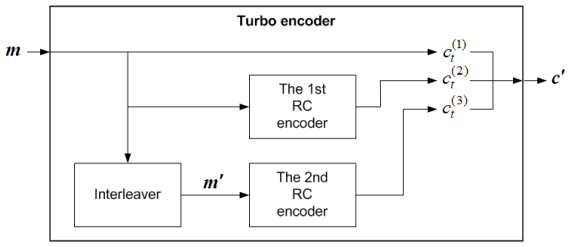

FIGURE 1. The block diagram of a systematic turbo encoder.

Notations: $(\cdot)^T$ and $(\cdot)^H$ stand for transpose and Hermitian transpose operations, respectively. $\lfloor x \rfloor$ denotes the greatest integer less than or equal to x. $|x|$ denotes the absolute value of x. With n being a natural number, $\mathcal{N}_n$ denotes a set given by $\{1, 2, \cdots, n\}$ and $n!$ denotes the factorization of n. diag($\mathbf{x}$) denotes a diagonal matrix with its diagonal components given by a vector $\mathbf{x}$. $\Re\{x\}$ and $\Im\{x\}$ denote the real and imaginary part of x, respectively. ${}_nC_k$ denotes the number of the k-combinations from a set of n components.

II. SYSTEM MODEL

We consider a turbo-coded OFDM-IQ-IM system operating in a frequency-selective channel environment. The OFDM block comprises N subcarriers and conveys a message $\mathbf{m}$ consisting of N_I information bits. We model the channel impulse response as a tapped delay line with $N/8$ taps, assuming that each channel tap has Rayleigh fading. Fig. 1 shows the block diagram of a systematic turbo encoder to generate systematic codes. We assume that the interleaver of the turbo encoder uses random interleaving. The turbo encoder triples the message $\mathbf{m}$ to yield a codeword $\mathbf{c}'$ that consists of $N_C (= 3N_I)$ bits. Then, the generated systematic code has a code rate $R_C = 1/3$. $\mathbf{m}'$ denote a sequence consisting of the interleaved bits of $\mathbf{m}$. m_t and m'_t for $t = 1, 2, \cdots, N_I$ denote the t-th bit of $\mathbf{m}$ and the t-th bit of $\mathbf{m}'$, respectively. $c_t^{(1)}$ is called systematic bit, which is the same as m_t. $c_t^{(2)}$ is the encoding result of m_t by the first recursive convolutional (RC) encoder and $c_t^{(3)}$ is the encoding result of m'_t by the second RC encoder. The encoded bits, $c_t^{(2)}$ and $c_t^{(3)}$, are called parity check bits. We assume that the first and second RC encoders have the same generation function given by

$$G(D) = (1 + D^2)/(1 + D + D^2), \tag{1}$$

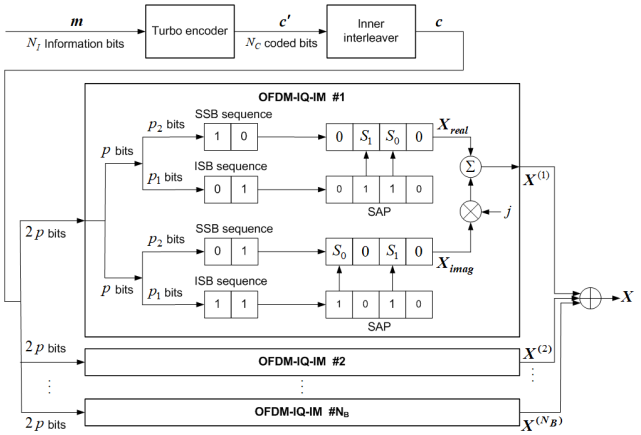

FIGURE 2. The transmitter structure of a turbo-coded OFDM-IQ-IM system with $n = 4$ and $k = 2$.

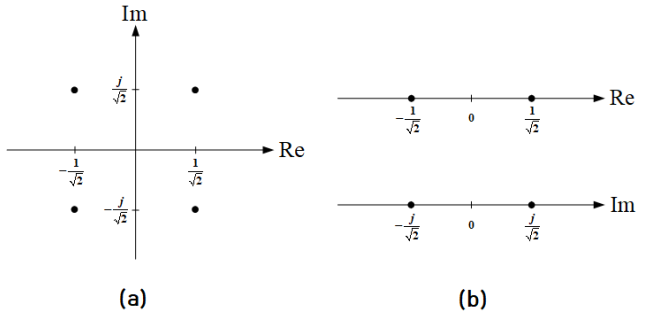

FIGURE 3. (a) The 4QAM symbol constellation, (b) The real and imaginary symbol constellations for a 4QAM-based OFDM-IQ-IM approach.

where D denotes the delay factor. The turbo-coded bit sequence $\mathbf{c}'$ of length $3N_I$ is formed as

$$\mathbf{c}' = [\, c_1^{(1)}\ c_1^{(2)}\ c_1^{(3)}\ c_2^{(1)}\ c_2^{(2)}\ c_2^{(3)}\ \cdots\ c_{N_I}^{(1)}\ c_{N_I}^{(2)}\ c_{N_I}^{(3)}\,]. \quad (2)$$

Fig. 2 shows the transmitter structure of a turbo-coded OFDM-IQ-IM system. The turbo-coded bit sequence $\mathbf{c}'$ is interleaved by an inner interleaver to yield $\mathbf{c}$. For OFDM-IQ-IM application, the OFDM block is divided into N_B subblocks and $\mathbf{c}$ is divided into N_B subsequences accordingly as

$$\mathbf{c} = [\, \mathbf{c}_1^T\ \mathbf{c}_2^T\ \cdots\ \mathbf{c}_{N_B}^T\,]^T, \quad (3)$$

where each subsequence carries N_C/N_B bits. The number of subcarriers in a subblock is $n = N/N_B$. OFDM-IQ-IM activates only k real subcarriers in a subblock to transmit k real symbols and only k imaginary subcarriers in a subblock to transmit k imaginary symbols. Symbols transmitted in a subblock are made up of the sum of the active real symbols selected from the real symbol constellation and the active imaginary symbols selected from the imaginary symbol constellation. In M-ary-QAM-based OFDM-IQ-IM, the number of the ISBs that can be transmitted in the real part of a subblock is $p_1 = \lfloor \log_2({}_nC_k) \rfloor$ and the number of the SSBs that can be transmitted in the real part of a subblock is $p_2 = k\lfloor \log_2(M)/2 \rfloor$. The same is true for the imaginary part of a subblock, so the total number of bits that can be transmitted in a subblock is $2(p_1+p_2)$. In M-ary-QAM-based OFDM, the number of the bits that can be transmitted on n subcarriers is $n\log_2(M)$. Therefore, with a fixed M, the condition for M-ary-QAM-based OFDM-IQ-IM to have a transmission rate greater than or equal to M-ary-QAM-based OFDM is given by

$$2(\lfloor \log_2({}_nC_k) \rfloor + k\lfloor \log_2(M)/2 \rfloor) \geq n\log_2(M). \quad (4)$$

The values of M that satisfy (4) for which (n,k) pairs exist are 2 and 4. In the case of $M = 4$, there are many pairs of (n, k) that satisfy this condition, i.e., (n, k)=(2, 1), (4, 2), (5, 2), (8, 3), (9, 3), (12, 4), $\cdots$, for the equality and (n, k)=(6, 3), (7, 3), (8, 4), (9, 4), (10, 4), (11, 4), $\cdots$, for the inequality.

However, when $M > 4$, there is no pair of (n, k) that satisfies the above condition. We choose $M = 4$ to compare the error rate performance of OFDM-IQ-IM and OFDM at the same transmission rate. 4QAM-based OFDM-IQ-IM prepares the real and imaginary symbol constellations by dividing the 4QAM symbol constellation as shown in Fig. 3. In this paper, we focus on a turbo-coded 4QAM-based OFDM-IQ-IM approach with $n = 2$ and $k = 1$, which corresponds to the simplest implementation with the same transmission rate as a turbo-coded 4QAM-based OFDM approach. We will show later in the simulation section that this approach outperforms the turbo-coded 4QAM-based OFDM approach in the high SNR region. In the turbo-coded 4QAM-based OFDM-IQ-IM approach with $n = 2$ and $k = 1$, the number of the bits carried in a subblock is given by $2(p_1 + p_2) = 2(1 + 1) = 4$. When $N = 120$, the number of the subblocks is $N_B = N/n = 60$ and the number of the turbo-coded bits is $N_C = 2p \times N_B = 240$. The bit sequence delivered in the β-th subblock for $\beta = 1, 2, \cdots, N_B$ is defined as

$$\mathbf{c}_\beta = \left[\, b_1,\ b_2,\ d_1,\ d_2\,\right]^T, \quad (5)$$

where b_1 and b_2 denote the ISBs and d_1 and d_2 denote the SSBs. b_1 is used to select an active real subcarrier and d_1 is used to select a real symbol transmitted over the active real subcarrier. Similarly, b_2 is used to select an active imaginary subcarrier and d_2 is used to select an imaginary symbol transmitted over the active imaginary subcarrier. The subcarrier activation pattern (SAP) sequence represents an active subcarrier pattern for a subblock. The total number of SAP sequences is given by $N_{\text{SAP}} = {}_2C_1 = 2$. According to [19] and [20], we assume that an SAP sequence, $\mathbf{a}_1 = [\,0, 1\,]$, is selected by an ISB 0 and another SAP sequence, $\mathbf{a}_2 = [\,1, 0\,]$, is selected by an ISB 1. Note that 0 and 1 in each of $\mathbf{a}_1$ and $\mathbf{a}_2$ denote inactive and active subcarriers, respectively. Let $\mathbf{a}_{\eta_1}$ and $\mathbf{a}_{\eta_2}$ for $\eta_1, \eta_2 \in \mathcal{N}_2$ be the SAPs that are used for transmitting the real and imaginary symbols, respectively. We denote the active real subcarrier index for transmitting the real symbol as $I_{\text{real}}^{(\eta_1)}$ and the active imaginary subcarrier index for transmitting the imaginary symbol as $I_{\text{image}}^{(\eta_2)}$. Note

that $I_{\text{real}}^{(\eta_1)}, I_{\text{image}}^{(\eta_2)} \in \mathcal{N}_2$. Defining

$$\mathcal{S} \triangleq \{S_0, S_1\} = \{-1/\sqrt{2},\ 1/\sqrt{2}\}, \tag{6}$$

we write the real and imaginary symbols transmitted on the active real and imaginary subcarriers of the β-th subblock as

$$\begin{aligned} X_{\text{real},I_{\text{real}}^{(\eta_1)}}^{(\beta)} &= S_{d_1}, \\ X_{\text{imag},I_{\text{imag}}^{(\eta_2)}}^{(\beta)} &= S_{d_2}, \end{aligned} \tag{7}$$

respectively. With $i_1 \neq I_{\text{real}}^{(\eta_1)}$ and $i_2 \neq I_{\text{imag}}^{(\eta_2)}$ for $i_1, i_2 \in \mathcal{N}_2$, we write $X_{\text{real},i_1}^{(\beta)} = 0$ and $X_{\text{imag},i_2}^{(\beta)} = 0$. Then, the symbol transmitted on the v-th subcarrier for $v \in \mathcal{N}_2$ is given by

$$X_v^{(\beta)} = X_{\text{real},v}^{(\beta)} + jX_{\text{imag},v}^{(\beta)}. \tag{8}$$

We define the OFDM block as

$$\mathbf{X} = \left[\, \mathbf{X}^{(1)^T}\ \mathbf{X}^{(2)^T}\ \cdots\ \mathbf{X}^{(N_B)^T} \,\right]^T, \tag{9}$$

where $\mathbf{X}^{(\beta)}$ denotes the β-th subblock,

$$\mathbf{X}^{(\beta)} = \left[\, X_1^{(\beta)}\ X_2^{(\beta)} \,\right]^T. \tag{10}$$

Since a subcarrier-level interleaver improves error performance by transforming a frequency domain channel into an uncorrelated one [27], we assume that $\mathbf{X}$ passes through a symbol-level interleaver to yield

$$\tilde{\mathbf{X}} = \left[\, X_1^{(1)} \cdots X_1^{(N_B)}\ X_2^{(1)} \cdots X_2^{(N_B)} \,\right]^T. \tag{11}$$

The interleaved OFDM block $\tilde{\mathbf{X}}$ undergoes inverse fast Fourier transform and cyclic prefix addition before transmission. At the receiver, a series of processes including cyclic prefix elimination, fast Fourier transform, and subcarrier-level deinterleaving are applied. Then, the received signal for the β-th subblock can be written as

$$\mathbf{Y}^{(\beta)} = \text{diag}\big(\mathbf{H}^{(\beta)}\big)\mathbf{X}^{(\beta)} + \mathbf{W}^{(\beta)}, \tag{12}$$

where $\mathbf{H}^{(\beta)}$ is the frequency domain channel vector

$$\mathbf{H}^{(\beta)} = \left[\, H_1^{(\beta)}\ H_2^{(\beta)} \,\right]^T \tag{13}$$

with $H_v^{(\beta)}$ for $v \in \mathcal{N}_2$ being a zero-mean circularly symmetric complex Gaussian (ZMCSCG) random variable with variance 0, and $\mathbf{W}^{(\beta)}$ is an additive noise vector

$$\mathbf{W}^{(\beta)} = \left[\, W_1^{(\beta)}\ W_2^{(\beta)} \,\right]^T \tag{14}$$

with $W_v^{(\beta)}$ for $v \in \mathcal{N}_2$ being a ZMCSCG random variable with variance N_0. The SNR is defined as $\rho = E_b/N_0$, where E_b denotes the average energy per bit. The v-th component of $\mathbf{Y}^{(\beta)}$ for $v \in \mathcal{N}_2$ can be written as

$$Y_v^{(\beta)} = H_v^{(\beta)} X_v^{(\beta)} + W_v^{(\beta)}. \tag{15}$$

The remaining receiver part of the turbo-coded OFDM-IQ-IM approach is illustrated in Fig. 4. By separating the posterior probability estimator block from the turbo decoder block, we decouple the turbo decoder design from the OFDM-IQ-IM demodulation design. Note that the turbo encoder block in Fig. 2 and the turbo decoder block in Fig. 4 can be easily replaced with other encoder and decoder blocks to apply different codes as long as the decoder can take the posterior probabilities of the coded bits as its input. The output of the posterior probability estimator corresponds to the posterior probabilities of ISBs and SSBs of OFDM-IQ-IM. The inner deinterleaver takes the output of the posterior probability estimator as its input and yields the posterior probabilities of turbo-coded bits. We assume that the BCJR decoding algorithm is used by the turbo decoder. The BCJR decoding algorithm requires as input the likelihood probabilities of turbo-coded bits. However, it is very difficult to derive the likelihood probabilities of turbo-coded bits because the ISBs and SSBs are tied together due to the nature of the IM application. We found that the posterior probabilities of turbo-coded bits can also be used as input to the BCJR decoding algorithm, which can be explained as follows.

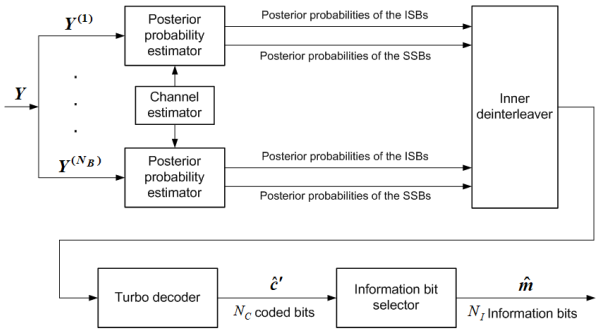

FIGURE 4. The receiver structure of a turbo-coded OFDM-IQ-IM system.

With the BCJR decoding algorithm, the prior probability that a systematic bit will be 0 (or 1) is initially set to 1/2, and the prior probability that an encoded parity check bit will be 0 (or 1) is also initially set to 1/2. According to Bayes' theorem [28], it can be said that the likelihood probability of a turbo-coded bit is proportional to the posterior probability of that bit in the initial stage of the BCJR decoding algorithm. For example, given $p(c_t^{(1)} = x) = 1/2$ for $x \in \{0, 1\}$, we can write the likelihood probability of $c_t^{(1)}$ as

$$p(r_t^{(1)}|c_t^{(1)} = x) = 2\,p(r_t^{(1)})\,p(c_t^{(1)} = x|r_t^{(1)}) \tag{16}$$

by the Bayes' theorem, where $r_t^{(1)}$ denotes the received signal corresponding to $c_t^{(1)}$. It means that the likelihood probability of $c_t^{(1)}$, $p(r_t^{(1)}|c_t^{(1)} = x)$, is proportional to the posterior probability of $c_t^{(1)}$, $p(c_t^{(1)} = x|r_t^{(1)})$. Since the BCJR decoding algorithm applies normalization to its input probabilities, the posterior probability of a turbo-coded bit can replace the likelihood possibility of that bit in the initial stage of the BCJR decoding algorithm. In the BCJR decoding algorithm, two decoders alternately and iteratively estimate the message sequence until the message sequences estimated by both decoders converge. Since each decoder uses the same set of likelihood possibilities of the systematic and encoded parity check bits for every iteration [29, chap. 14], it is concluded that the posterior probabilities of turbo-coded bits can be

taken as input to the turbo decoder and used iteratively for every iteration of the BCJR decoding algorithm.

The posterior probability estimator calculates the posterior probabilities of ISBs and SSBs of OFDM-IQ-IM for all sub-blocks and sends the results to the inner deinterleaver. The formulas to calculate the posterior probabilities of ISBs and SSBs of OFDM-IQ-IM are presented in Appendix-A. Finally, the turbo decoder estimates $\mathbf{c}'$ by using the output of the inner deinterleaver and extracts the systematic bits from the estimated $\mathbf{c}'$ to estimate the message $\hat{\mathbf{m}}$.

III. PROPOSED SCHEME

We describe an efficient bit mapping scheme for a turbo-coded OFDM-IQ-IM approach without puncturing, followed by an efficient bit mapping scheme for a turbo-coded OFDM-IQ-IM approach with puncturing. We investigate the difference in error rate between systematic bits and parity check bits of systematic turbo coding and the difference in error rate between ISBs and SSBs of OFDM-IQ-IM. Based on the results, we devise a new bit mapping scheme.

A. FOR THE CASE WHERE NO PUNCTURING IS USED

We assume that the length of the message $\mathbf{m}$ is $N_I = 80$, the length of the rate 1/3 turbo-code $\mathbf{c}'$ is $N_C = 240$, and the number of ISBs and SSBs is 120 each.

1) THE RANDOM BIT MAPPING SCHEME WHEN NO PUNCTURING IS APPLIED

For the case when no puncturing is applied, we consider the following random bit mapping scheme. In the inner interleaver block as shown in Fig. 2, the turbo-coded bit sequence $\mathbf{c}'$ in (2) is divided into three subsequences,

$$\begin{aligned}\mathbf{c}'^{(1)} &= [\, c_1^{(1)}\ c_2^{(1)}\ \cdots\ c_{N_I}^{(1)}\,],\\ \mathbf{c}'^{(2)} &= [\, c_1^{(2)}\ c_2^{(2)}\ \cdots\ c_{N_I}^{(2)}\,],\\ \mathbf{c}'^{(3)} &= [\, c_1^{(3)}\ c_2^{(3)}\ \cdots\ c_{N_I}^{(3)}\,].\end{aligned} \tag{17}$$

The lengths of $\mathbf{c}'^{(1)}$, $\mathbf{c}'^{(2)}$, and $\mathbf{c}'^{(3)}$ are 80, respectively. Then, $\mathbf{c}'^{(1)}$, $\mathbf{c}'^{(2)}$, and $\mathbf{c}'^{(3)}$ are merged into a sequence according to random interleaving. The ISBs and SSBs are taken alternatively in order from the merged sequence and finally, $\mathbf{c}$ is formed according to (3) and (5). When the receiver is done estimating the posterior probabilities of the bits of $\mathbf{c}$, it finds the posterior probabilities of the bits of $\mathbf{c}'$ by performing the opposite operations of the inner interleaver on the posterior probabilities of the bits of $\mathbf{c}$.

2) THE ERROR RATE DIFFERENCE BETWEEN THE SYSTEMATIC BITS AND PARITY CHECK BITS OF TURBO CODES

We divide the turbo-coded bit sequence $\mathbf{c}'$ into three subsequences, $\mathbf{c}'^{(1)}$, $\mathbf{c}'^{(2)}$, and $\mathbf{c}'^{(3)}$ as in (17). We examine which subsequence is more susceptible to errors by forcing intentional errors on the posterior probabilities of the bits of each subsequence and applying the BCJR algorithm. To craft

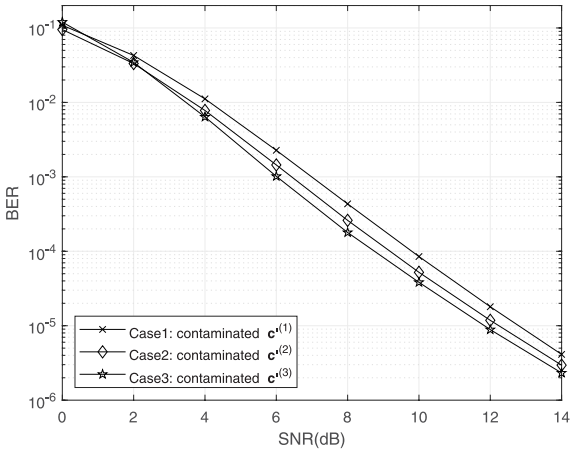

FIGURE 5. BER comparison of three intentional error cases when considering the turbo-coded 4QAM-based OFDM-IQ-IM approach.

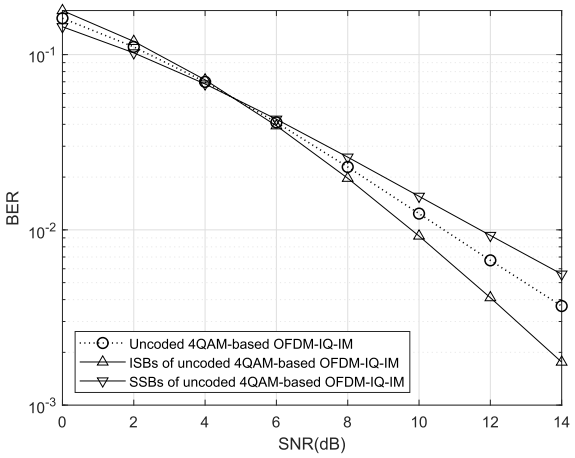

FIGURE 6. BER comparison of the ISBs, the SSBs, and the entire bits of the uncoded 4QAM-based OFDM-IQ-IM approach.

intentional errors to a subsequence, we select 8 (i.e., 10 %) bits out of the subsequence, set the posterior probability of each selected bit to 0.999 if the posterior probability of that bit is less than 0.5, and set the posterior probability of each selected bit to 0.001 if the posterior probability of that bit is greater than 0.5. We compare three cases; in Case 1, the posterior probabilities of the 8 selected bits of $\mathbf{c}'^{(1)}$ are corrupted with intentional errors, in Case 2, the posterior probabilities of the 8 selected bits of $\mathbf{c}'^{(2)}$ are corrupted with intentional errors, and in Case 3, the posterior probabilities of the 8 selected bits of $\mathbf{c}'^{(3)}$ are corrupted with intentional errors. Fig. 5 presents the BER curves of the three cases when considering the turbo-coded 4QAM-based OFDM-IQ-IM approach. It can be seen that Case 1 performs worse than Case 2 and Case 3 in all SNR region. The reason is that the posterior probabilities of the bits of $\mathbf{c}'^{(1)}$ are used by both decoders in the BCJR algorithm, but the posterior probabilities of the bits of $\mathbf{c}'^{(2)}$ or $\mathbf{c}'^{(3)}$ are only used by one decoder in the BCJR algorithm. That is, the errors in the posterior probabilities of the bits of $\mathbf{c}'^{(1)}$ affect both decoders

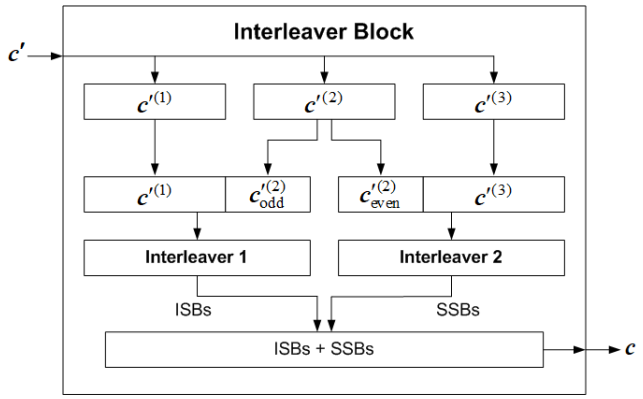

FIGURE 7. The proposed bit mapping scheme when no puncturing is applied.

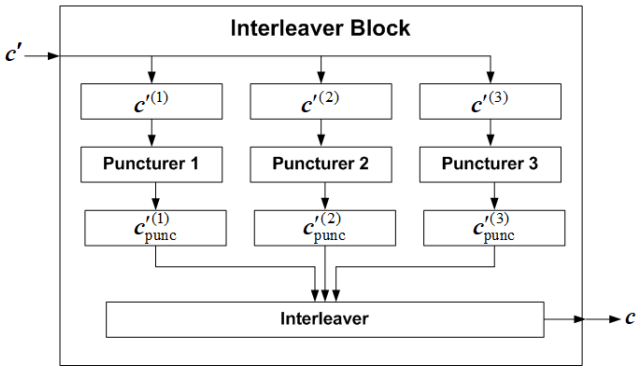

FIGURE 8. The first conventional interleaving scheme for the case where the puncturing is evenly applied to all turbo-coded bits.

of the BCJR algorithm, further degrading the performance of the turbo decoder. It can also be seen that Case 2 performs worse than Case 3. Since errors can propagate and expand through iterative decoding, the first decoding by the first decoder is more critical than the second decoding by the second decoder in the BCJR algorithm. In the experimental simulation, we assume that the first decoder of the BCJR algorithm takes as input the posterior probabilities of the bits of $\mathbf{c}'^{(2)}$ and that the second decoder of the BCJR algorithm takes as input the posterior probabilities of the bits of $\mathbf{c}'^{(3)}$. Therefore, errors in the posterior probabilities of the bits of $\mathbf{c}'^{(2)}$ degrade the performance of the turbo decoder more than errors in the posterior probabilities of the bits of $\mathbf{c}'^{(3)}$. These results suggest that protecting $\mathbf{c}'^{(1)}$ from error is most critical to improving the overall performance of the turbo-coded 4QAM-based OFDM-IQ-IM approach and that protecting $\mathbf{c}'^{(2)}$ from error is more critical than protecting $\mathbf{c}'^{(3)}$ from error.

3) THE ERROR RATE DIFFERENCE BETWEEN THE ISBs AND SSBs OF OFDM-IQ-IM

For OFDM-IQ-IM, the input bits are split into two sets of bits; the set of the ISBs and the set of the SSBs. We examine which set of bits is more robust to errors when considering an uncoded 4QAM-based OFDM-IQ-IM approach. Fig. 6 presents the BER curves of the ISBs and the SSBs when considering an uncoded 4QAM-based OFDM-IQ-IM approach. For reference, the BER curve from the entire bits of the uncoded 4QAM-based OFDM-IQ-IM approach is also included. It can be seen that the ISBs attain better BER performance than the SSBs at SNRs higher than 4.8dB. This observation is consistent with the derivation result of the pairwise error probability for an OFDM-IM system in [4], which showed that at a high SNR the diversity order of index bits is greater than the diversity order of symbol bits.

Combining these experimental results with the experimental results given in the previous subsection, we can conclude that to improve the performance of the turbo-coded 4QAM-based OFDM-IQ-IM approach in the high SNR region, it is necessary to use as many bits of $\mathbf{c}'^{(1)}$ and $\mathbf{c}'^{(2)}$ as possible for ISB purposes.

4) THE PROPOSED BIT MAPPING SCHEME

Based on the results found in the previous subsections, we propose a new bit mapping scheme for a turbo-coded 4QAM-based OFDM-IQ-IM approach without the puncturing. Fig. 7 shows the bit mapping scheme we propose for the case where no puncturing is used. The turbo-coded bit sequence $\mathbf{c}'$ is divided into three subsequences, $\mathbf{c}'^{(1)}$, $\mathbf{c}'^{(2)}$, and $\mathbf{c}'^{(3)}$, as in (17). $\mathbf{c}'^{(2)}$ is divided into odd-indexed and even-indexed subsequences, $\mathbf{c}'^{(2)}_{\text{odd}}$ and $\mathbf{c}'^{(2)}_{\text{even}}$, each of which is of length 40. To use as many bits of $\mathbf{c}'^{(1)}$ and $\mathbf{c}'^{(2)}$ as possible for ISB purposes, the bits of $\mathbf{c}'^{(1)}$ and $\mathbf{c}'^{(2)}_{\text{odd}}$ are used as the ISBs and the bits of $\mathbf{c}'^{(3)}$ and $\mathbf{c}'^{(2)}_{\text{even}}$ are used as the SSBs. Specifically, the sequence of the ISBs is formed by merging $\mathbf{c}'^{(1)}$ and $\mathbf{c}'^{(2)}_{\text{odd}}$ according to random interleaving and the sequence of the SSBs is formed by merging $\mathbf{c}'^{(3)}$ and $\mathbf{c}'^{(2)}_{\text{even}}$ according to random interleaving. Finally, $\mathbf{c}$ is formed by merging the ISB and SSB sequences according to (3) and (5). Note that the proposed bit mapping scheme is for implementing the inner interleaver block as shown in Fig. 2. Since the proposed bit mapping scheme can be implemented without changing the internal structures of the turbo encoder and decoder, it can be realized at low cost.

B. FOR THE CASE WHERE THE PUNCTURING IS USED

Next, we consider the case where a rate $1/3$ turbo-code is punctured to generate a rate $1/2$ turbo-code. The procedure for designing high-rate turbo-codes via puncturing was presented in the literature such as [30] and [31]. We assume that the length of the message $\mathbf{m}$ is $N_I = 120$, the length of the rate 1/3 turbo-code $\mathbf{c}'$ is $N_C = 360$, and the length of the rate 1/2 turbo-code $\mathbf{c}$ obtained after puncturing $\mathbf{c}'$ is 240. Note that puncturing is performed such that the bit of $\mathbf{c}'$ at the position of 0 in the puncturing pattern is omitted.

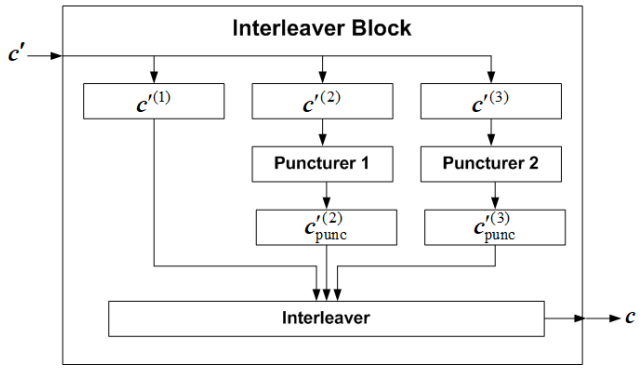

FIGURE 9. The second conventional interleaving scheme for the case where the puncturing is applied only to the parity check bits.

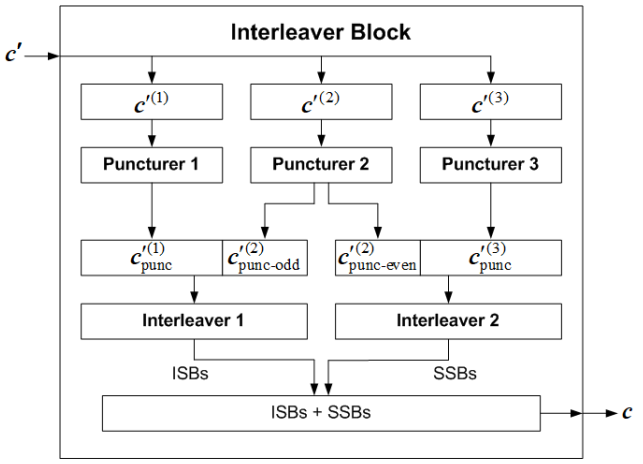

FIGURE 10. The proposed bit mapping scheme for the case where the puncturing is used.

1) THE FIRST RANDOM BIT MAPPING SCHEME FOR THE CASE WHERE THE PUNCTURING IS EVENLY APPLIED TO ALL TURBO-CODED BITS

We consider a random bit mapping scheme as shown in Fig. 8. Note that this scheme is to implement the inner interleaver block for the case where the puncturing is evenly applied to all turbo-coded bits. The turbo-coded bit sequence $\mathbf{c}'$ is divided into three subsequences, $\mathbf{c}'^{(1)}$, $\mathbf{c}'^{(2)}$, and $\mathbf{c}'^{(3)}$, each of which is of length 120. $\mathbf{c}'^{(1)}$, $\mathbf{c}'^{(2)}$, and $\mathbf{c}'^{(3)}$ are punctured with puncturing patterns, [0 1 1], [1 0 1], and [1 1 0] to yield $\mathbf{c}'^{(1)}_{\text{punc}}$, $\mathbf{c}'^{(2)}_{\text{punc}}$, and $\mathbf{c}'^{(3)}_{\text{punc}}$, respectively. Then, $\mathbf{c}'^{(1)}_{\text{punc}}$, $\mathbf{c}'^{(2)}_{\text{punc}}$, and $\mathbf{c}'^{(3)}_{\text{punc}}$ are merged into a sequence according to random interleaving. The ISBs and SSBs are taken alternatively in order from the merged sequence and finally, $\mathbf{c}$ is formed according to (3) and (5). When the receiver is done estimating the posterior probabilities of the bits of $\mathbf{c}$, it finds the posterior probabilities of the bits of $\mathbf{c}'^{(1)}_{\text{punc}}$, $\mathbf{c}'^{(2)}_{\text{punc}}$, and $\mathbf{c}'^{(3)}_{\text{punc}}$ by performing the opposite operations of the inner interleaver on the posterior probabilities of the bits of $\mathbf{c}$. Then, it inserts 0.5 at every punctured positions of $\mathbf{c}'^{(1)}_{\text{punc}}$, $\mathbf{c}'^{(2)}_{\text{punc}}$, and $\mathbf{c}'^{(3)}_{\text{punc}}$ to retrieve the posterior probabilities of the bits of $\mathbf{c}'$.

2) THE SECOND RANDOM BIT MAPPING SCHEME FOR THE CASE WHERE THE PUNCTURING IS APPLIED ONLY TO THE PARITY CHECK BITS

For punctured turbo code design, it is often used to apply predetermined puncturing to the parity check bits of a good turbo code [30]. Therefore, we consider another random bit mapping scheme as shown in Fig. 9. Note that this scheme is to implement the inner interleaver block for the case where the puncturing is applied only to the parity check bits. The turbo-coded bit sequence $\mathbf{c}'$ is divided into three subsequences, $\mathbf{c}'^{(1)}$, $\mathbf{c}'^{(2)}$, and $\mathbf{c}'^{(3)}$, each of which is of length 120. $\mathbf{c}'^{(2)}$ and $\mathbf{c}'^{(3)}$ are punctured with puncturing patterns, [1 0] and [0 1], to yield $\mathbf{c}'^{(2)}_{\text{punc}}$ and $\mathbf{c}'^{(3)}_{\text{punc}}$, respectively. Then, $\mathbf{c}'^{(1)}$, $\mathbf{c}'^{(2)}_{\text{punc}}$, and $\mathbf{c}'^{(3)}_{\text{punc}}$ are merged into a sequence according to random interleaving. The ISBs and SSBs are taken alternatively in order from the merged sequence and finally, $\mathbf{c}$ is formed according to (3) and (5). When the receiver is done estimating the posterior probabilities of the bits of $\mathbf{c}$, it finds the posterior probabilities of the bits of $\mathbf{c}'^{(1)}$, $\mathbf{c}'^{(2)}_{\text{punc}}$, and $\mathbf{c}'^{(3)}_{\text{punc}}$ by performing the opposite operations of the inner interleaver on the posterior probabilities of the bits of $\mathbf{c}$. Then, it inserts 0.5 at every punctured positions of $\mathbf{c}'^{(2)}_{\text{punc}}$ and $\mathbf{c}'^{(3)}_{\text{punc}}$ to retrieve the posterior probabilities of the bits of $\mathbf{c}'$.

3) THE ERROR RATE DIFFERENCE BETWEEN THE SYSTEMATIC BITS AND PARITY CHECK BITS OF PUNCTURED CODES

The error rate difference between the systematic bits and parity check bits of punctured codes can be investigated in the same way as in III-A2. Since the result is very similar to that presented in Fig. 5, it is omitted here. The same conclusion can be reached through this experimental simulation. To improve the performance of the turbo-coded 4QAM-based OFDM-IQ-IM approach in the high SNR region, it is necessary to use as many bits of $\mathbf{c}'^{(1)}$ and $\mathbf{c}'^{(2)}$ as possible for ISB purposes.

4) THE PROPOSED BIT MAPPING SCHEME

Fig. 10 shows the bit mapping scheme we propose for the case where the puncturing is used. The turbo-coded bit sequence $\mathbf{c}'$ is divided into three subsequences, $\mathbf{c}'^{(1)}$, $\mathbf{c}'^{(2)}$, and $\mathbf{c}'^{(3)}$, each of which is of length 120. Then, $\mathbf{c}'^{(1)}$, $\mathbf{c}'^{(2)}$, and $\mathbf{c}'^{(3)}$ are punctured with puncturing patterns, [0 1 1], [1 0 1], and [1 1 0] to yield $\mathbf{c}'^{(1)}_{\text{punc}}$, $\mathbf{c}'^{(2)}_{\text{punc}}$, and $\mathbf{c}'^{(3)}_{\text{punc}}$, respectively. $\mathbf{c}'^{(2)}_{\text{punc}}$ is divided into odd-indexed and even-indexed subsequences, $\mathbf{c}'^{(2)}_{\text{punc-odd}}$ and $\mathbf{c}'^{(2)}_{\text{punc-even}}$, each of which is of length 40. The sequence of the ISBs is formed by merging $\mathbf{c}'^{(1)}_{\text{punc}}$ and $\mathbf{c}'^{(2)}_{\text{punc-odd}}$ according to random interleaving and the sequence of the SSBs is formed by merging $\mathbf{c}'^{(3)}_{\text{punc}}$ and $\mathbf{c}'^{(2)}_{\text{punc-even}}$ according to random interleaving. Finally, $\mathbf{c}$ is formed by merging the ISB and SSB sequences according to (3) and (5).

IV. DISCUSSION

In this section, we will compare the difference in turbo-decoding complexity between the turbo-coded

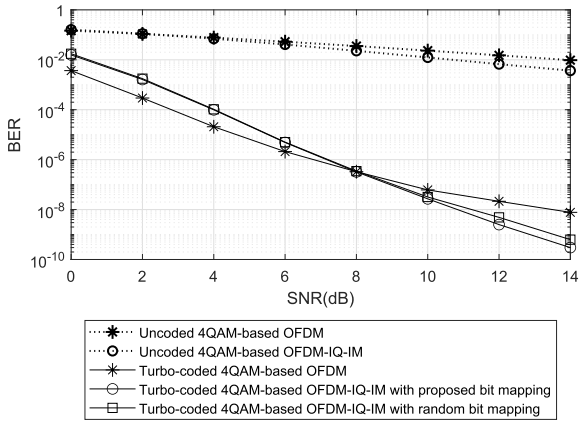

FIGURE 11. BER comparison of the proposed bit mapping and other schemes when considering the turbo-coded 4QAM-based OFDM-IQ-IM approach without puncturing.

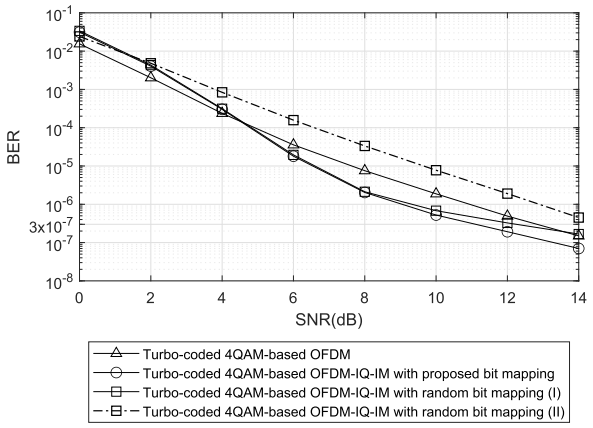

FIGURE 12. BER comparison of the proposed bit mapping and other schemes when considering the turbo-coded 4QAM-based OFDM-IQ-IM approach with puncturing.

4QAM-based OFDM-IQ-IM approach and the turbo-coded 4QAM-based OFDM. The difference in turbo-decoding complexity comes mostly from computing the posterior probabilities of turbo-coded bits. Therefore, as a figure of merit for comparing turbo-decoding complexity, we consider the numbers of real multiplications (RMs) and real additions (RAs) required to compute the posterior probabilities of turbo-coded bits transmitted on n subcarriers. In computing the numbers of RMs and RAs, we use the following rules introduced in [22]: one complex multiplication converts to 4 RMs and 2 RAs, one complex addition converts to 2 RAs, and one operation of $|\cdot|^2$ converts to 2 RMs and 1 RA. The turbo-coded M-ary-QAM-based OFDM-IQ-IM approach requires $2^{p_1} \times 9n(p_1 + 2p_2)$ RMs and $2^{p_1} \times 4n(p_1+2p_2)+2(2n-1)(p_1+p_2)$ RAs, where $p_1 = \lfloor \log_2({}_nC_k) \rfloor$ and $p_2 = k\lfloor \log_2(M)/2 \rfloor$. The turbo-coded M-ary-QAM-based OFDM approach requires $6nM \times \log_2(M)$ RMs and $2n(3M-1) \times \log_2(M)$ RAs. In the case of $M = 4$, $n = 2$, and $k = 1$, the former approach requires 108 RMs and 60 RAs, whereas the latter approach requires 96 RMs and 88 RAs. Therefore, it can be said that the turbo-decoding complexity of the turbo-coded 4QAM-based OFDM-IQ-IM approach with $n = 2$ and $k = 1$ is similar to that of the turbo-coded 4QAM-based OFDM approach.

V. SIMULATION RESULTS

In Fig. 11, the proposed bit mapping scheme described in III-A4 is compared to the random bit mapping scheme described in III-A1 when considering a turbo-coded 4QAM-based OFDM-IQ-IM approach with $n = 2$, $k = 1$, $N = 120$, and $N_I = 80$. For reference, the BER curve of a turbo-coded 4QAM-based OFDM approach, that of an uncoded 4QAM-based OFDM approach, and that of an uncoded 4QAM-based OFDM-IQ-IM approach are also included in the figure. It is seen that the uncoded 4QAM-based OFDM-IQ-IM approach outperforms the uncoded 4QAM-based OFDM approach at SNRs higher than 4dB. The gain of the uncoded 4QAM-based OFDM-IQ-IM approach over uncoded 4QAM-based OFDM approach is 3dB at BER 10^{-2}. It is also seen that the turbo-coded 4QAM-based OFDM-IQ-IM approach applying the proposed bit mapping scheme outperforms the turbo-coded 4QAM-based OFDM approach at SNRs higher than 8dB. The gain of the turbo-coded 4QAM-based OFDM-IQ-IM approach applying the proposed bit mapping scheme over the turbo-coded 4QAM-based OFDM approach is 2.2dB at BER 10^{-8}. Since both approaches transmit the same number of message bits in the OFDM block, it is concluded that the turbo-coded 4QAM-based OFDM-IQ-IM approach is superior to the turbo-coded 4QAM-based OFDM approach in the high SNR region. The reason why the turbo-coded 4QAM-based OFDM-IQ-IM scheme is inferior to the turbo-coded 4QAM-based OFDM scheme in the low SNR region can be explained as follows. At a low SNR, OFDM-IQ-IM receivers make more errors in detecting active subcarrier patterns because the noise power on inactive subcarriers is high while the power of symbols transmitted on active subcarriers is low. As a result, ISBs generate more detection errors, and subsequently SSBs also generate more errors. For this reason, the turbo-coded 4QAM-based OFDM-IQ-IM approach performs worse than the turbo-coded 4QAM-based OFDM approach in the low SNR region. Finally, it is seen that the proposed bit mapping scheme improves the performance of the turbo-coded 4QAM-based OFDM-IQ-IM approach more than the random bit mapping scheme for all SNR region. The SNR gain of the proposed bit mapping scheme over the random bit mapping scheme is 0.5dB at BER 10^{-9}. This gain proves the effectiveness of the proposed bit mapping scheme. This performance improvement can be obtained by designing only the inner interleaver block without changing the internal structures of the turbo encoder and decoder.

In Fig. 12, the proposed bit mapping scheme described in III-B4 is compared to the two random bit mapping schemes described in III-B1 and of III-B2 when considering a punctured 4QAM-based OFDM-IQ-IM approach with $n = 2$, $k = 1$, $N = 120$, and $N_I = 120$. For reference, the BER curve of a punctured 4QAM-based OFDM approach is also included in the figure. It is seen that the punctured

4QAM-based OFDM-IQ-IM approach applying the proposed bit mapping scheme outperforms the punctured 4QAM-based OFDM approach at SNRs higher than 4.75dB. The gain of the punctured 4QAM-based OFDM-IQ-IM approach applying the proposed bit mapping scheme over the punctured 4QAM-based OFDM approach is 2.3dB at BER 10^{-6}. It is also seen that the punctured 4QAM-based OFDM-IQ-IM approach applying the proposed bit mapping scheme outperforms the punctured 4QAM-based OFDM-IQ-IM approach applying one of the two random bit mapping schemes for all SNR region. The SNR gain of the proposed bit mapping scheme over the first random bit mapping scheme is 1dB at BER 3×10^{-7} and the SNR gain of the proposed bit mapping scheme over the second random bit mapping scheme is 1.75dB at BER 10^{-4}. These gains prove the efficiency of the proposed bit mapping scheme when the turbo code rate is increased by puncturing.

VI. CONCLUSION

We presented a decoupled design of an OFDM-IQ-IM demodulator and a turbo decoder to apply turbo coding to OFDM-IQ-IM. We proposed a bit mapping scheme that can efficiently split turbo-coded bits into the ISBs and SSBs of OFDM-IQ-IM. The proposed bit mapping scheme improved the performance of the turbo-coded 4QAM-based OFDM-IQ-IM approach compared to random bit mapping schemes in all SNR region. In addition, the turbo-coded 4QAM-based OFDM-IQ-IM approach applying the proposed bit mapping scheme outperformed the turbo-coded 4QAM-based OFDM approach in the high SNR region. Since the proposed bit mapping scheme can be implemented without changing the internal structures of the turbo encoder and decoder, it has the advantage that it can be realized at low cost.

APPENDIX A

The formulas to calculate the LLRs of the ISBs and SSBs of OFDM-IQ-IM can be similarly derived as in [23], which derived formulas for OFDM-IM. We focus on the β-th sub-block. In (5), b_1 and b_2 denote the ISBs. The LLR of b_1 is given by

$$\lambda_1 = \min_{\mathbf{a}_\eta \in \mathcal{A}_{b_1=0}} \sum_{m \in \mathcal{N}_n} \min_{s \in \mathcal{S}} \Phi_{\text{real}}^{(\beta)}(m, s) - \min_{\mathbf{a}_\eta \in \mathcal{A}_{b_1=1}} \sum_{m \in \mathcal{N}_n} \min_{s \in \mathcal{S}} \Phi_{\text{real}}^{(\beta)}(m, s), \tag{18}$$

where $\mathcal{A}_{b_1=x}$ for $x \in \{0, 1\}$ denotes the set of the SAP sequences satisfying the condition of $b_1 = x$ and

$$\Phi_{\text{real}}^{(\beta)}(m, s) = \left|H_m^{(\beta)}\right|^2 \cdot \left|\Re\{Y_m^{(\beta)}/H_m^{(\beta)}\} - s \cdot a_{\eta,m}\right|^2 / N_0. \tag{19}$$

The LLR of b_2 is also given by (18) if λ_1 is replaced with λ_2, b_1 is replaced with b_2, and $\Phi_{\text{real}}^{(\beta)}(m, s)$ is replaced with

$$\Phi_{\text{imag}}^{(\beta)}(m, s) = \left|H_m^{(\beta)}\right|^2 \cdot \left|\Im\{Y_m^{(\beta)}/H_m^{(\beta)}\} - s \cdot a_{\eta,m}\right|^2 / N_0. \tag{20}$$

In (5), d_1 and d_2 denote the SSBs. The LLR of d_1 is given by

$$\bar{\lambda}_1 = \min_{\mathbf{a}_\eta \in \mathcal{A}} \left\{ \Phi_{\text{real}}^{(\beta)}(I_{\text{real}}^{(\eta)}, S_0) + \sum_{m \in \mathcal{N}_n, m \neq I_{\text{real}}^{(\eta)}} \min_{s \in \mathcal{S}} \Phi_{\text{real}}^{(\beta)}(m, s) \right\} - \min_{\mathbf{a}_\eta \in \mathcal{A}} \left\{ \Phi_{\text{real}}^{(\beta)}(I_{\text{real}}^{(\eta)}, S_1) + \sum_{m \in \mathcal{N}_n, m \neq I_{\text{real}}^{(\eta)}} \min_{s \in \mathcal{S}} \Phi_{\text{real}}^{(\beta)}(m, s) \right\}, \tag{21}$$

where $\mathcal{A}$ denotes the set of all the 2^{p_1} SAP sequences. The LLR of d_2 is also given by (21) if $\bar{\lambda}_1$ is replaced with $\bar{\lambda}_2$, d_1 is replaced with d_2, $I_{\text{real}}^{(\eta)}$ is replaced with $I_{\text{imag}}^{(\eta)}$, and $\Phi_{\text{real}}^{(\beta)}(\cdot)$ is replaced with $\Phi_{\text{imag}}^{(\beta)}(\cdot)$. Provided with λ_v for $v = 1, 2$, the posterior probability of b_v can be computed by

$$p(b_v = 1|\mathbf{Y}^{(\beta)}) = \frac{1}{e^{-\lambda_v} + 1} \tag{22}$$

and

$$p(b_v = 0|\mathbf{Y}^{(\beta)}) = 1 - p(b_v = 1|\mathbf{Y}^{(\beta)}). \tag{23}$$

Provided with $\bar{\lambda}_v$, the posterior probabilities of d_v can also be computed by (22) and (23) if b_v and λ_v are replaced with d_v and $\bar{\lambda}_v$, respectively.

REFERENCES

[1] E. Basar, M. Wen, R. Mesleh, M. Di Renzo, Y. Xiao, and H. Haas, "Index modulation techniques for next-generation wireless networks," *IEEE Access*, vol. 5, pp. 16693–16746, 2017.

[2] S. D. Tusha, A. Tusha, E. Basar, and H. Arslan, "Multidimensional index modulation for 5G and beyond wireless networks," *Proc. IEEE*, vol. 109, no. 2, pp. 170–199, Feb. 2021.

[3] P. K. Frenger and N. A. B. Svensson, "Parallel combinatory OFDM signaling," *IEEE Trans. Commun.*, vol. 47, no. 4, pp. 558–567, Apr. 1999.

[4] E. Başar, U. Aygölü, E. Panayırcı, and H. V. Poor, "Orthogonal frequency division multiplexing with index modulation," *IEEE Trans. Signal Process.*, vol. 61, no. 22, pp. 5536–5549, Nov. 2013.

[5] B. Zheng, F. Chen, M. Wen, F. Ji, H. Yu, and Y. Liu, "Low-complexity ML detector and performance analysis for OFDM with in-phase/quadrature index modulation," *IEEE Commun. Lett.*, vol. 19, no. 11, pp. 1893–1896, Nov. 2015.

[6] R. Fan, Y. J. Yu, and Y. L. Guan, "Generalization of orthogonal frequency division multiplexing with index modulation," *IEEE Trans. Wireless Commun.*, vol. 14, no. 10, pp. 5350–5359, Oct. 2015.

[7] M. Wen, B. Ye, E. Basar, Q. Li, and F. Ji, "Enhanced orthogonal frequency division multiplexing with index modulation," *IEEE Trans. Wireless Commun.*, vol. 16, no. 7, pp. 4786–4801, Jul. 2017.

[8] Q. Li, M. Wen, E. Basar, H. V. Poor, B. Zheng, and F. Chen, "Diversity enhancing multiple-mode OFDM with index modulation," *IEEE Trans. Commun.*, vol. 66, no. 8, pp. 3653–3666, Aug. 2018.

[9] T. Mao, Z. Wang, Q. Wang, S. Chen, and L. Hanzo, "Dual-mode index modulation aided OFDM," *IEEE Access*, vol. 5, pp. 50–60, 2017.

[10] M. Wen, E. Basar, Q. Li, B. Zheng, and M. Zhang, "Multiple-mode orthogonal frequency division multiplexing with index modulation," *IEEE Trans. Commun.*, vol. 65, no. 9, pp. 3892–3906, Sep. 2017, doi: 10.1109/TCOMM.2017.2710312.

[11] J. Li, S. Dang, M. Wen, X.-Q. Jiang, Y. Peng, and H. Hai, "Layered orthogonal frequency division multiplexing with index modulation," *IEEE Syst. J.*, vol. 13, no. 4, pp. 3793–3802, Dec. 2019.

[12] R. Mesleh, S. S. Ikki, and H. M. Aggoune, "Quadrature spatial modulation," *IEEE Trans. Veh. Technol.*, vol. 64, no. 6, pp. 2738–2742, Jun. 2015.

[13] J. Li, M. Wen, X. Cheng, Y. Yan, S. Song, and M. Ho Lee, "Generalized precoding-aided quadrature spatial modulation," *IEEE Trans. Veh. Technol.*, vol. 66, no. 2, pp. 1881–1886, Feb. 2017.

[14] E. Başar, "OFDM with index modulation using coordinate interleaving," *IEEE Wireless Commun. Lett.*, vol. 4, no. 4, pp. 381–384, Aug. 2015.

[15] Y. Liu, F. Ji, H. Yu, F. Chen, D. Wan, and B. Zheng, "Enhanced coordinate interleaved OFDM with index modulation," *IEEE Access*, vol. 5, pp. 27504–27513, 2017.
[16] M. Wen, Q. Li, E. Basar, and W. Zhang, "Generalized multiple-mode OFDM with index modulation," *IEEE Trans. Wireless Commun.*, vol. 17, no. 10, pp. 6531–6543, Oct. 2018.
[17] M. Wen, J. Li, S. Dang, Q. Li, S. Mumtaz, and H. Arslan, "Joint-mapping orthogonal frequency division multiplexing with subcarrier number modulation," *IEEE Trans. Commun.*, vol. 69, no. 7, pp. 4306–4318, Jul. 2021.
[18] J. Li, S. Dang, Y. Huang, P. Chen, X. Qi, M. Wen, and H. Arslan, "Composite multiple-mode orthogonal frequency division multiplexing with index modulation," *IEEE Trans. Wireless Commun.*, early access, Nov. 9, 2022, doi: 10.1109/TWC.2022.3220752.
[19] X. Li, H. Wang, N. Guan, and W. Lai, "A dual-mode index modulation scheme with gray-coded pairwise index mapping," *IEEE Commun. Lett.*, vol. 22, no. 8, pp. 1580–1583, Aug. 2018.
[20] E. Yoon, S.-Y. Kim, S. Kwon, and U. Yun, "An efficient index mapping algorithm for OFDM-index modulation," *IEEE Access*, vol. 7, pp. 184194–184206, 2019.
[21] H. Zhang, L.-L. Yang, and L. Hanzo, "LDPC-coded index-modulation aided OFDM for in-vehicle power line communications," in *Proc. IEEE 83rd Veh. Technol. Conf. (VTC Spring)*, Nanjing, China, May 2016, pp. 1–5.
[22] X. Yu and J. Pang, "Performance evaluation of OFDM index modulation with LDPC code," in *Proc. IEEE 31st Annu. Int. Symp. Pers., Indoor Mobile Radio Commun.*, London, U.K., Sep. 2020, pp. 1–5.
[23] E. Yoon, S. Kwon, U. Yun, and S.-Y. Kim, "LDPC decoding with low complexity for OFDM index modulation," *IEEE Access*, vol. 9, pp. 68435–68444, 2021.
[24] Q. Shi, N. Wu, H. Wang, X. Ma, and L. Hanzo, "Factor graph based message passing algorithms for joint phase-noise estimation and decoding in OFDM-IM," *IEEE Trans. Commun.*, vol. 68, no. 5, pp. 2906–2921, May 2020.
[25] L. Wei and J. Zheng, "Approximate message passing-aided iterative channel estimation and data detection of OFDM-IM in doubly selective channels," *IEEE Access*, vol. 7, pp. 133410–133420, 2019.
[26] L. Bahl, J. Cocke, F. Jelinek, and J. Raviv, "Optimal decoding of linear codes for minimizing symbol error rate," *IEEE Trans. Inf. Theory*, vol. IT-20, no. 2, pp. 284–287, Mar. 1974.
[27] Y. Xiao, S. Wang, L. Dan, X. Lei, P. Yang, and W. Xiang, "OFDM with interleaved subcarrier-index modulation," *IEEE Commun. Lett.*, vol. 18, no. 8, pp. 1447–1450, Aug. 2014.
[28] J. Joyce, "Bayes' theorem," in *The Stanford Encyclopedia of Philosophy*, E. N. Zalta, Ed. Stanford, CA, USA: Stanford Univ., The Metaphysics Research Lab, Philosophy Department, Fall 2003. [Online]. Available: http://plato.stanford.edu/entries/bayes-theorem/
[29] T. K. Moon, *Error Correction Coding*. Hoboken, NJ, USA: Wiley-InterScience, 2005.
[30] C. Berrou and A. Glavieux, "Near optimum error correcting coding and decoding: Turbo-codes," *IEEE Trans. Commun.*, vol. 44, no. 10, pp. 1261–1271, Oct. 1996.
[31] K. Aksoy and Ü. Aygölü, "New punctured turbo codes," *AEU Int. J. Electron. Commun.*, vol. 57, no. 3, pp. 206–213, Jan. 2003.

EUNCHUL YOON (Senior Member, IEEE) received the B.S. and M.S. degrees in electronics engineering from Yonsei University, Seoul, South Korea, in 1993 and 1995, respectively, and the Ph.D. degree in electrical engineering from Stanford University, Stanford, CA, USA, in 2005. From February 1995 to July 2000, he was with the Samsung CDMA System Development Team, Seoul, where he was involved in the design of system software. From December 2005 to February 2008, he was with the Samsung WiMAX System Development Group, Suwon, South Korea, where he developed the modem methods for beamforming and MIMO. Since March 2008, he has been with the Department of Electrical and Electronics Engineering, Konkuk University, Seoul. His research interests include wireless networks, coding and modulation, interference cancelation, and deep learning for wireless communications.

SOONBUM KWON is currently pursuing the degree with the Department of Electrical and Electronics Engineering, Konkuk University, Seoul, South Korea. His research interests include wireless networks, coding and modulation, interference cancelation, and deep learning for wireless communications.

SUN YONG KIM (Senior Member, IEEE) received the B.S.E. (summa cum laude), M.S.E., and Ph.D. degrees in electrical engineering from the Korea Advanced Institute of Science and Technology (KAIST), Daejeon, in 1990, 1993, and 1995, respectively. From April 1995 to March 1996, he was a Visiting Researcher with The University of Tokyo, Tokyo, Japan. From March 1996 to August 2001, he was with the Department of Electronics Engineering, Hallym University. In September 2001, he joined the Department of Electrical and Electronics Engineering, Konkuk University, where he is currently a Professor. His research interests include detection and estimation theory, statistical signal processing, and analysis and design of mobile communication systems. He won the Second-Best Paper Award from the IEEE Korea Section, in 1990, the Scholarship from the IEEE Communication Society, from 1992 to 1993, and a Paper Award from the LG Information and Communications, in 1994.